Cancer Letters 490 (2020) 100–110

Contents lists available at ScienceDirect

Cancer Letters

journal homepage: www.elsevier.com/locate/canlet

Endothelial cells under therapy-induced senescence secrete CXCL11, which increases aggressiveness of breast cancer cells

Hyun Jung Hwang [a,b], Ye-Rim Lee [a,b], Donghee Kang [a,b], Hyung Chul Lee [a,b], Haeng Ran Seo [c], Ji-Kan Ryu [a,d], Yong-Nyun Kim [e], Young-Gyu Ko [f], Heon Joo Park [a,g], Jae-Seon Lee [a,b,*]

[a] Hypoxia-related Disease Research Center, Inha University College of Medicine, Incheon, South Korea
[b] Department of Molecular Medicine, Inha University College of Medicine, Incheon, South Korea
[c] Cancer Biology Research Laboratory, Institute Pasteur Korea, Gyeonggi-do, South Korea
[d] Department of Urology, Inha University College of Medicine, Incheon, South Korea
[e] Division of Translational Research, Research Institute, National Cancer Center, Goyang, 10408, South Korea
[f] Division of Life Sciences, Korea University, Seoul, South Korea
[g] Department of Microbiology, Inha University College of Medicine, Incheon, South Korea

ARTICLE INFO

Keywords:
Therapy-induced senescence
Endothelial cells
Tumor microenvironment
CXCL11

ABSTRACT

The effects of senescence associated secretory phenotype (SASP) from therapy-induced senescent endothelial cells on tumor microenvironment (TME) remains to be clarified. Here, we investigated effects of ionizing radiation (IR)- and doxorubicin-induced senescent HUVEC on TME. MDA-MB-231 cancer cells treated with conditioned medium (CM) from senescent HUVEC or co-cultured with senescent HUVEC significantly increased cancer cell proliferation, migration, and invasion. We found that CXCL11 plays a principal role in the senescent CM-induced aggressive activities of MDA-MB-231 cells. When we treated HUVEC with a neutralizing anti-CXCL11 antibody or CXCL11 SiRNA, or treated MDA-MB-231 cells with CXCR3 SiRNA, we observed synergistic diminution of the ability of the HUVEC SASP to alter the migration and spheroid invasion of cancer cells. ERK activation was involved in the HUVEC SASP-induced aggressive activity of MDA-MB-231 cells. Finally, we observed the *in vivo* effect of CXCL11 from the senescent HUVEC in tumor-bearing mice. Together, our results demonstrate that SASP from endothelial cells experiencing therapy-induced senescence promotes the aggressive behavior of cancer cells, and that CXCL11 can potentially be targeted to prevent the adverse effects of therapy-induced senescent endothelial cells on the tumor microenvironment.

1. Introduction

Cellular senescence was originally identified as a permanent exit from the cell cycle after a finite number of cell divisions, such as seen in cultured human fibroblasts [1,2]. Today, senescence is regarded as a stress response that can be promoted by a wide range of intrinsic and extrinsic stimuli, including oncogenic activation, oxidative and genotoxic stress, mitochondrial dysfunction, irradiation, and chemotherapeutic agents [3]. Compared with proliferating cells, senescent cells display an enlarged morphology, distinct metabolic and gene expression patterns, and increased activity of lysosomal β-galactosidase [4]. Another typical characteristic of senescent cells is the secretion of a myriad of proteins [5,6]. For example, senescent cells secrete IL-6 and IL-8, which are inflammatory cytokines that recruit inflammatory cells [6–8], and matrix metalloproteinases (MMP), which alter the extracellular matrix [9,10]. This phenomenon is called the senescence-associated secretory phenotype (SASP) and has been shown to influence neighboring cells and cause changes in the tissue microenvironment [11].

Cellular senescence is required for developmental morphogenesis, wound repair, prevention of organ fibrosis, and tumor suppression in young individuals [12–15]. However, as senescent cells accumulate in tissues with advancing age, this cellular phenotype contributes to age-related diseases, such as cataracts, sarcopenia, and atherosclerosis [13,16]. The age-associated accumulation of senescent cells has been connected to the increased levels of SASP factors, which are related to chronic inflammation and arthritis [15,17,18]. SASP factors have also been shown to elevate inflammatory responses, stimulate the growth of

* Corresponding author. Department of Molecular Medicine, Inha University College of Medicine, Incheon, 22212, South Korea.
E-mail address: jaeslee@inha.ac.kr (J.-S. Lee).

https://doi.org/10.1016/j.canlet.2020.06.019
Received 6 November 2019; Received in revised form 18 June 2020; Accepted 22 June 2020
Available online 11 July 2020

nearby malignant cells, and promote the metastasis of malignant cancer cells [9,19,20]. Moreover, the SASP has been shown to lead to the epithelial mesenchymal transition (EMT), which is a phenomenon that stimulates cancer cell motility [10].

Tumor development is a process that involves the co-evolution of transformed cells and the tumor microenvironment (TME) [21]. The TME includes numerous non-cancerous cell types, including fibroblasts, endothelial cells, and infiltrating lymphocytes [22]. Many studies have demonstrated that the TME plays critical roles in various aspects of tumor progression (i.e., tumor angiogenesis, proliferation, invasion, and metastasis) and also mediates therapeutic resistance [23–25]. However, little is known about the effects of therapy-induced senescent endothelial cells on cancer progression.

In this study, we examined the effect of SASP from therapy-induced senescent human umbilical vein endothelial cells (HUVEC). From these cells, we identified CXCL11 as a promising therapeutic target that is associated with aggressive features of cancer cells in the TME.

2. Materials and methods

2.1. Cell culture

MDA-MB-231 cells, MDA-MB-453 cells, HCC70 cells and MCF-10A cells were purchased from American Type Culture Collection (ATCC). MDA-MB-231, MDA-MB-453, and HCC70 cells were grown in RPMI-1640 (WelGENE, Inc., Daegu, Korea). MCF-10A cells were cultured in DMEM/F12 (WelGENE) containing 5% horse serum and freshly supplemented with insulin, epidermal growth factor, hydrocortisone, and cholera toxin. Human umbilical vein endothelial cells (HUVEC) and endothelial colony forming cells (ECFC) were grown in EBM-2 (Lonza, Walkersville, MD, USA) supplemented with 2% FBS, hFGF-B, VEGF, R3-IGF-1, hEGF, hydrocortisone, ascorbic acid, heparin, gentamicin, and amphotericin-B (Lonza). Human dermal microvascular endothelial cells (HMVEC) were cultured in EGM2-MV using a bullet kit (Lonza).

2.2. Reagents and antibodies

Anti-pRb, anti-phospho-pRb, and anti-cleaved PARP antibodies were purchased from Cell Signaling Technology (Danvers, MA, USA). Anti-p53 antibody was purchased from Leica Biosystems (Wetzlar, Germany). Anti-p21 antibody was purchased from Santa Cruz Biotechnology (Santa Cruz, CA, USA). Anti-actin antibody was purchased from ABM (Richmond, BC, Canada). Anti-CXCL11 antibody was purchased from R&D Systems (Minneapolis, MN, USA). Anti-CD31 antibody was purchased from Thermo Fisher Scientific (Waltham, MA, USA). Anti-N-cadherin, anti-E-cadherin, anti-slug, and anti-vimentin antibodies were purchased Abcam (Cambridge, UK).

2.3. Irradiation

Cells were irradiated with an X-RAD iR160 X-ray irradiator (Precision X-ray (PXi) Inc., North Branford, CT, USA) with a 2-mm Al filter, an accelerating voltage of 150 kV, and a dose rate of 0.72 Gy/min.

2.4. Senescence-associated β-galactosidase staining

Cells were washed with 1x phosphate-buffered saline (PBS), fixed in 3.7% formaldehyde, washed, and incubated for 16 h at 37 °C with a solution containing 1 mg/ml of 5-bromo-4-chloro-3-indolyl B-D-galactoside (X-Gal), 40 mM citric acid/sodium phosphate, pH 6.0, 5 mM potassium ferrocyanide, 5 mM potassium ferricyanide, 150 mM NaCl, and 2 mM $MgCl_2$. The samples were washed, and the cell staining was photographed using a microscope (Olympus CKX41; Olympus).

2.5. Collection of conditioned media (CM)

Endothelial cells (HUVEC, HMVEC, or ECFC) were seeded at 5×10^5 cells/ml in 100-mm culture dishes, cultured overnight, and exposed to either radiation (6 Gy) or doxorubicin (50 ng/ml). The cells were cultured in a CO_2 incubator for 2 days, washed with PBS, and then incubated in serum-free medium. After 24 h, CM was collected and centrifuged for 5 min at 3000 rpm to remove cell debris. The supernatant was concentrated 5-fold with a Centricon-10 concentrator (Millipore, Billerica, MA, USA) and centrifuged at 3000 rpm for 100 min at 4 °C. The volume of the collected CM was normalized with respect to the number of cells in the dish from which it was collected.

2.6. Immunoblot analysis

Cell lysates were prepared in RIPA lysis buffer containing protease inhibitors (Roche, Basel, Switzerland) and phosphatase inhibitors (Sigma-Aldrich). Equal amounts of proteins were subjected to sodium dodecyl sulfate polyacrylamide gel electrophoresis (SDS-PAGE). The proteins were transferred to a nitrocellulose membrane, and the membrane was blocked with 3% non-fat dried milk or 3% BSA, and incubating with primary antibodies at 4 °C overnight. After incubation with horseradish peroxidase (HRP)-conjugated secondary antibodies for 1 h, the membrane was processed with enhanced chemiluminescence reagents (Thermo Fisher Scientific) and exposed to X-ray film (Agfa Gevaert NV, Mortsel, Antwerp, Belgium).

2.7. Cell viability

Cells were seeded in 60-mm dishes, cultured for 24 h, and treated with CM as indicated in the figures. After 3 days, cells were trypsinized and harvested. Cell viability was measured with a trypan blue exclusion assay. Cell suspensions were diluted 1:1 with 0.4% trypan blue (GIBCO, Grand Island, NY, USA) and the cells were counted with a hemocytometer under a microscope (Olympus CKX41; Olympus).

2.8. BrdU incorporation assay

Cell proliferation was measured using a 5-bromo-2′-deoxy-uridine (BrdU) Cell Proliferation Assay Kit (Roche Applied Science) according to the manufacturer's instructions. BrdU incorporation was determined spectrophotometrically by measuring absorbance at 450 nm.

2.9. In vitro cell migration and invasion assays

Transwell migration and Matrigel invasion assays were conducted using the methods described by the manufacturer (Costar, Cambridge, MA, USA). We used modified Boyden chambers with 8-μm pore filter inserts for 24-well plates (Costar). For the transwell migration assay, 1×10^5 cells in 200 μl medium were added to the upper chamber and 600 μl of CM was placed in the lower chamber. Cells were incubated at 37 °C under 5% CO_2. For the invasion assay, the filters were pre-coated with 10 μl ice cold 10% Matrigel (BD Biosciences, San Jose, CA, USA) in cold Dulbecco's phosphate buffered saline (DPBS), and all other steps were performed as described for the transwell migration assay. After 16 h, the cells that had migrated through the filter were fixed with 3.7% formaldehyde solution for 10 min and stained with 0.1% crystal violet solution for 10 min. The cells that remained on the upper surface were removed with cotton swabs. Images of the stained cells were captured, and the cells were counted using a light microscope (Olympus CKX41; Olympus, Shinjuku, Tokyo, Japan).

2.10. Wound-healing assay

Cells were seeded on 24-well plates and allowed to reach confluence overnight. A 200-μL pipette tip was used to make a scratch in the cell

monolayer. The cells were washed twice with PBS and incubated in CM at 37 °C in a CO_2 incubator. After 16 h, the cells were washed with DPBS, fixed with 3.7% formaldehyde for 10 min at room temperature, and were stained with 0.1% crystal violet staining solution (Sigma-Aldrich). Images were obtained under a microscope (Olympus CKX41; Olympus), and the cell migration activity was assessed according to the percentage of the area that was repaired.

2.11. RNA interference

Cells were transfected with 100 nM siRNA duplexes by using RNAiMAX (Invitrogen, Karlsruhe, Germany). The sequences of the siRNA (Bioneer Inc., Daejeon, Korea) were as follows:

Con Si (5′-CCUACGCCACCAAUUUCGUdTdT-3′)
CXCL11 Si (5′-GAGAACAUUUCUGUCUCUAdTdT-3′)
CXCL11 Si #2 (5′-GUGGUUACGGUGGAGACAdTdT-3′)
CXCL11 Si #3 (5′-CAAUAUGUAGGGAGACAUUdTdT-3′)
CCL2 Si (5′-CUCCGAAGACUUGAACACUdTdT-3′)
CXCL16 Si (5′-GCACCUGACUCUAAUACCUdTdT-3′)
INHBA Si (5′-CACAGUGCCAAUACCAUGAdTdT-3′)
CXCR3 Si (5′-UAGAGACAGAAAUGUUCUCdTdT-3′)

2.12. Plasmid transfection

Transfection of plasmids was conducted using Lipofectamine 2000 reagent (Invitrogen) according to the manufacturer's instructions. The plasmid expressing the Flag-tagged CXCL11 was purchased from OriGene (Rockville, MD, USA).

2.13. Reverse transcription-quantitative polymerase chain reaction

Total RNA was extracted using the TRIzol reagent (Invitrogen) according to the manufacturer's instructions and re-suspended in diethyl pyrocarbonate water. After reverse transcription (RT) using the cDNA synthesis kit (Bio-Medical Science Co. Ltd, Daejeon, Korea), PCR was performed using gene-specific primers. RT-quantitative polymerase chain reaction (PCR) was performed using the iQ™ SYBR® Green Supermix (Bio-Rad Laboratories, Hercules, CA, USA) on a CFX Connect™ Real-Time PCR Detection System (Bio-Rad Laboratories). Each reaction volume of 16 μL contained SYBR® Green Super Mix, cDNA template, and primers. Pre-designed qRT-PCR primers were purchased from Bioneer Co., Ltd (Daejeon, Korea).

2.14. RNA-seq processing and analysis

Total RNA was isolated from HUVEC using the TRIzol reagent, dissolved in RNase-free water, and sequenced using an Illumina HiSeq 2000 (LAS Inc., Gimpo, Korea). The abundance of each transcript was quantified as fragments per kilobases of transcripts per million of mapped reads (FPKMs). The thresholds were set using the absolute value of log 2 (fold change) with FPKM $\geq$1.5 to determine significant differences in gene expression. The DAVID gene annotation tool (version 6.8; http://david.ncifcrf.gov/) was used for gene ontology analysis of the gene sets of interest.

2.15. Tube-formation assay

Matrigel (BD Biosciences) was polymerized (200 μL/well of a 48-well tissue culture plate) for 30 min at 37 °C. Trypsinized HUVEC (4×10^4) were resuspended in 200 μl of CM and seeded to each well. After 16 h, images showing tube morphology were photographed under a microscope. The numbers of branch points and branches were counted, and the tube area was measured using the Fuji Multi Gauge V2.3 software (Fuji, Tokyo, Japan).

2.16. Spheroid-invasion assay

Cells suspended in complete medium were seeded at a density of 5×10^3 cells/well in 96-well round-bottom ultra-low attachment microplates (Corning B.V. Life Sciences, Amsterdam, Netherlands) and incubated at 37 °C in 5% CO_2. For the formation of mixed-cell spheroids containing cancer cells and endothelial cells, MDA-MB-231 cells and HUVEC were mixed at a 1:1 ratio. The spheroids were allowed to form for 3 days, whereupon 100 μl of cold 7.5 mg/ml Matrigel basement membrane matrix (Corning) was loaded carefully into each spheroid-containing well, on ice. The plate was incubated for up to 96 h and the spheroids were photographed under a light microscope (Olympus CKX41; Olympus, Shinjuku, Tokyo, Japan) and analyzed using the ImageJ software (version 10.2; NIH, Bethesda, MD, USA).

2.17. Animal experiments

To observe the induction of endothelial cell senescence by radiation, MDA-MB-231 cells (2×10^6) were injected subcutaneously into the right hind legs of 5-week-old BALB/c nude mice from (Orientbio, Sungnam, Korea). When the tumors reached a volume of 100 mm^3, mice right hind legs were exposed to 12 Gy of IR by mouse shields (PXi Inc.; XD1907-2022) and sacrificed 5 days later. Excised tumors were fixed for immunohistochemical analysis. For the xenograft tumor growth assay, MDA-MB-231 cells (2×10^6) were injected subcutaneously into the right flank of nude mice. When the tumors reached a volume of 50 mm^3, mice were intratumorally injected every other day with 20-fold concentrated CM harvested from proliferating HUVEC (Con CM) or IR-exposed HUVEC (IR CM) with or without CXCL11 Si treatment. Calipers were used to measure the length (L) and width (W) of each subcutaneous tumor. The tumor volume (TV) was calculated as: $TV = (L \times W2)/2$. All animal care and experimental procedures were conducted in accordance with the guidance for animal experiments edited by Inha University (Incheon, Korea).

2.18. Immunohistochemistry

Tissues were cryosectioned at 20 μm thickness, fixed with 3.7% formaldehyde and permeabilized with 0.01% Triton-X100 for 15 min. The samples were then blocked with 3% BSA for 1 h at room temperature and incubated with primary antibody diluted in blocking solution overnight at 4 °C. As primary antibodies (diluted 1:50), we used rat anti-CD31 (Thermo Fisher Scientific), anti-p53 (Leica), and anti-p21 (Santa Cruz). Sections were washed in PBS and incubated with secondary antibodies diluted in blocking solution for 1 h at room temperature. The utilized secondary antibodies were Alexa Fluor 594 goat anti-hamster IgG (Jackson ImmunoResearch Laboratories, West Grove, PA, USA; 1:50), Alexa Fluor 488 goat anti-rabbit, and Alexa Fluor 488 goat anti-mouse (Jackson ImmunoResearch Laboratories; 1:50). The sections were washed three times with PBS and mounted on microscopy slides.

2.19. Statistical analysis

Statistical values are expressed as the mean ± SD. Statistical analysis was performed using the One-way ANOVA or *t* tests. Significance levels were set at $p < 0.05$.

3. Results

3.1. Ionizing radiation and doxorubicin treatment effectively induce premature senescence in various types of endothelial cells

To study the effects of senescent endothelial cells on cancer cells during cancer therapy, we firstly examined whether endothelial cells effectively become senescent following irradiation or doxorubicin treatment. Indeed, exposure to 6 Gy of IR or 50 ng/ml of doxorubicin

(Doxo) induced premature senescence in HUVEC, which was characterized by analysis of typical senescence phenotypes, such as pRb hypophosphorylation, p53/p21 accumulation, decreased cell number, and SA-β-Gal positivity (Fig. 1A and B). The cells did not show PARP cleavage, an apoptosis marker (Fig. 1A and B). IR- or Doxo-induced premature senescence phenotypes were also observed in other types of endothelial cells, including HMVEC (human microvascular endothelial cells) and umbilical cord blood-derived endothelial cells, as well as in the so-called ECFC (endothelial colony-forming cells) (Supplementary Fig. S1). We previously reported that 12 Gy of IR exposure induces cancer cell senescence in tumor tissues of xenograft mice [26]. To test whether radiation exposure induces premature senescence in endothelial cells *in vivo*, we irradiated tumor tissue of xenograft mice with 12 Gy of IR and used immunohistochemistry to examine the localization of CD31 (an endothelial cell marker) and p53/p21 (senescence markers) (Fig. 1C). We found that irradiated tumor tissues exhibited evident p53/p21 expression, and that this signal co-localized with that of CD31. In contrast, non-irradiated tumor tissues exhibited CD31 expression alone, without that of p53/p21.

3.2. SASP of therapy-induced senescent endothelial cells affects the migration and invasion activities of MDA-MB-231 cells

To investigate the effect of senescent endothelial cells on the TME, we collected CM (5-fold concentrated) from proliferating (Con), IR-, and Doxo-induced (therapy-induced) senescent HUVEC and applied these CM to MDA-MB-231 human mammary cancer cells and MCF-10A human mammary epithelial cells. A BrdU cell proliferation assay revealed that CM from both IR- and Doxo-induced senescent HUVEC dramatically increased the proliferation of MDA-MB-231 cells. In contrast, senescent HUVEC CM-treated MCF-10A cells did not show any evident increase in cell proliferation (Supplementary Fig. S2A). For each experimental group, the corresponding MDA-MB-231 and MCF-10A cells were incubated in serum-free medium and 10% serum-containing medium as negative and positive controls, respectively. To confirm this finding, we measured relative cell numbers following senescent

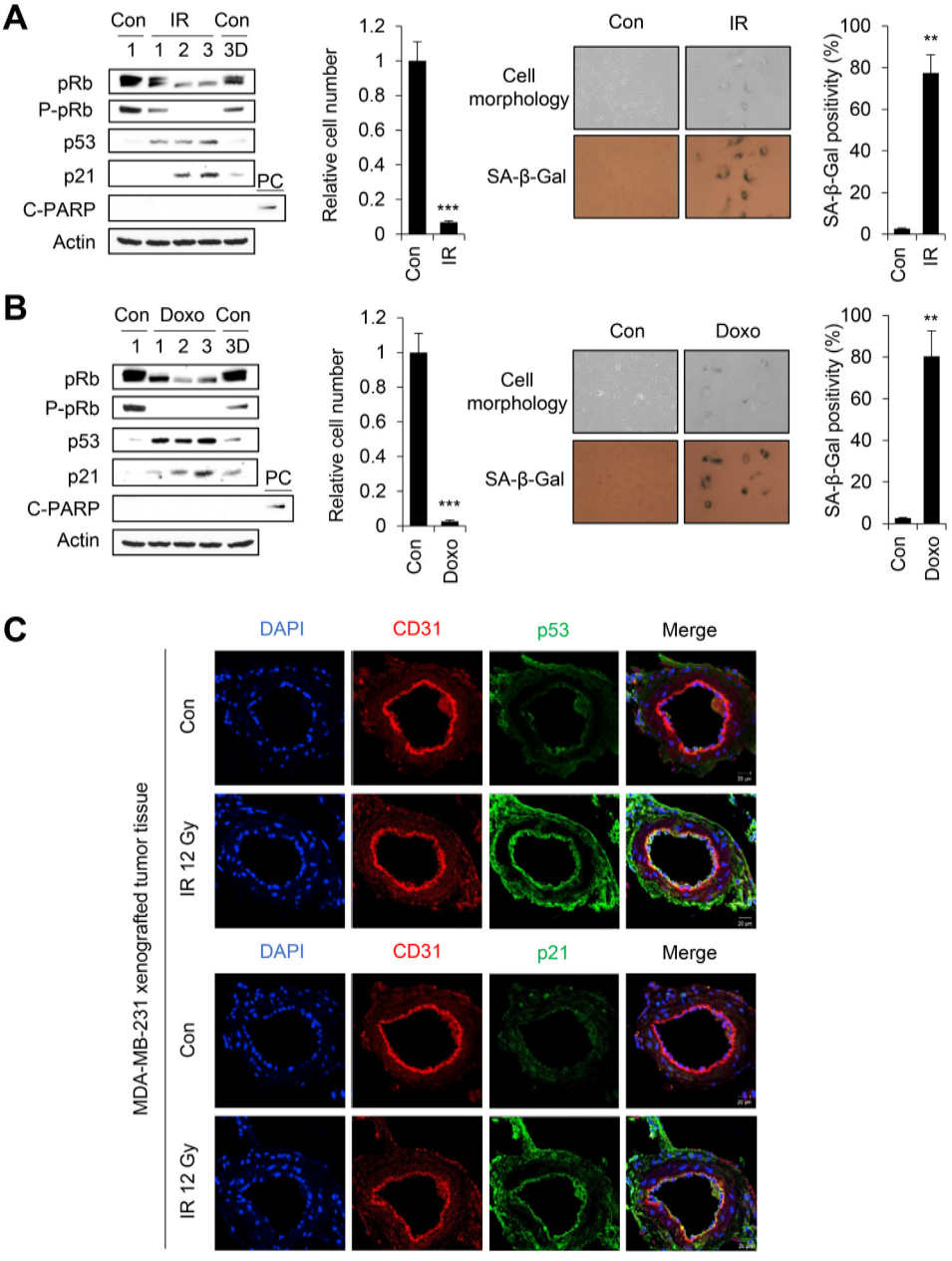

Fig. 1. Ionizing radiation and doxorubicin induce endothelial cell senescence in vitro and in vivo. (A, B) HUVEC exposed to 6 Gy of IR (A) or 50 ng/ml of doxorubicin (B) were subjected to immunoblotting and SA-β-Gal activity assays. Relative cell numbers and SA-β-Gal-positive cells were quantitated. (C) Tumor tissues of xenograft mice injected with MDA-MB-231 cells were locally exposed to 12 Gy of IR, and the expression levels of CD31, p53, and p21 in tumor tissues were detected by immunofluorescence.

HUVEC CM-treatment and under co-culture (Supplementary Figs. S2B–C). Indeed, we found that senescent HUVEC CM effectively increased the relative cell numbers in MDA-MB-231 cells, but not in MCF-10A cells. A wound-healing assay revealed that the SASP of therapy-induced senescent HUVEC increased the wound-healing activity of MDA-MB-231 cells but not MCF-10A cells (Fig. 2A). Consistent results were obtained in the co-culture wound-healing assay (Fig. 2B). CM from senescent HMVEC and senescent ECFC induced by IR or doxorubicin also increased the migratory activity of MDA-MB-231 cells, but not MCF-10A cells (Supplementary Figs. S3A–B). These results indicate that SASP of senescent endothelial cells affected to MDA-MB-231 cancer cells, but not so significantly to MCF-10A normal epithelial cells. We next investigated how the SASP of senescent HUVEC affected cell invasiveness. An invasion assay revealed that senescent HUVEC CM significantly increased the invasiveness of MDA-MB-231 cells (Fig. 2C). We observed increased expression of N-cadherin, Slug, and Vimentin and decreased expression of E-cadherin (EMT-related molecular changes) in MDA-MB-231 cells treated with senescent HUVEC CM (Fig. 2D). We also found that CM from senescent HMVEC and ECFC increased the invasiveness of MDA-MB-231 cells (Supplementary Figs. S3C–D). Since MCF-10A cells are relatively non-invasive, we did not conduct an invasion assay using these cells. Together, these results suggest that SASP from three different endothelial cell lines (HUVEC, HMVEC, and ECFC) commonly increases the migratory and invasive activities of MDA-MB-231 cells.

To identify the possible effects of senescent endothelial cell CM on angiogenesis, we performed a tube-formation assay. For the negative and positive control groups, Matrigel was overlaid with HUVEC suspended in serum-free medium or medium containing 0.1% serum and growth factors (VEGF, EGF, FGF and IGF), respectively. Our results indicated that the branch point number, branch number, and tube area were not altered by senescent HUVEC CM treatment (Supplementary Fig. S4A). Moreover, endothelial cells incubated with senescent HUVEC CM or control medium for 3 days showed no significant difference in endothelial cell division (Supplementary Fig. S4B).

3.3. Analysis of the senescent HUVEC SASP

To identify cytokines that are differentially expressed in senescent HUVEC, we induced senescence by exposing HUVEC to 6 Gy of IR and analyzed cytokine profiles using the next-generation sequencing (NGS)

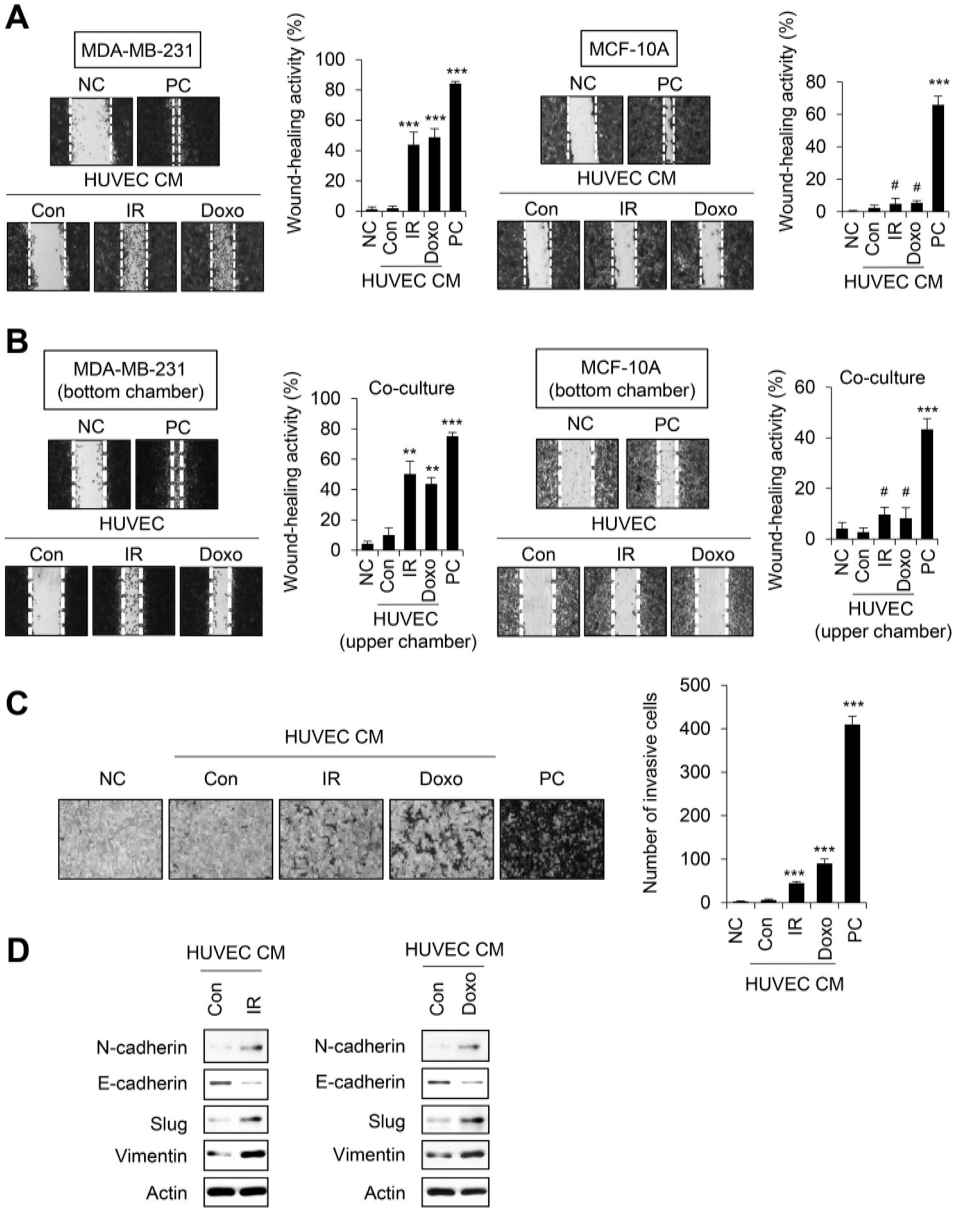

Fig. 2. Effects of senescent HUVEC CM on cell migration and invasion in MDA-MB-231 and MCF-10A cells. (A-D) MDA-MB-231 or MCF-10A cells were treated with 5-fold concentrated CM collected from proliferative HUVEC (Con), IR-, and Doxo-treated senescent HUVEC. After 24 h of CM treatment, we performed a wound-healing assay (A), co-culture wound-healing assay (B), invasive activity assay (C), and immunoblotting (D). For the negative control (NC) and positive control (PC) groups, cells were incubated in serum-free medium and medium containing 1% serum, respectively. The values represent the mean ± SD; n = 3; #P > 0.05; **P < 0.01; ***P < 0.001.

technique. The heatmap in Fig. 3A shows the top 17 cytokines whose expression levels were increased in IR-induced senescent HUVEC. We confirmed the expression changes of 10 of these genes by RT-PCR (Fig. 3B). To verify which cytokine plays important role on TME, HUVEC were transfected with each indicated siRNA (Si) and subjected to irradiation, and MDA-MB-231 cells were treated with harvested CM from HUVEC and assessed for their migratory activity (Fig. 3C). Our results revealed that IR-induced senescent CM from CXCL11 Si-treated HUVEC had the strongest effect on the migratory activity of MDA-MB-231 cells. Thus, we selected CXCL11 for further analysis. To confirm the secretion of CXCL11, we irradiated HUVEC with 6 Gy of IR and analyzed cell lysates (WCL) and CM (Fig. 3D). We observed a time-dependent increase of CXCL11 expression in WCL and CM. Furthermore, we investigated whether the expression of CXCL11 is increased in irradiated tumor tissues *in vivo*. We irradiated tumor tissues of xenograft mice with 12 Gy of IR and analyzed the expression levels of CD31 and CXCL11 by immunohistochemistry. CXCL11 was significantly increased and highly co-localized with CD31 in irradiated tumor tissues (Fig. 3E). When senescent HUVEC were treated with a neutralizing anti-CXCL11 antibody (Neut-anti-CXCL11), the obtained CM failed to show the effects of IR-induced senescent HUVEC CM on the wound-healing and migratory activity of MDA-MB-231 cells (Fig. 3F).

3.4. CXCL11 from senescent HUVEC CM promotes migratory and invasive activities through the receptor, CXCR3, and the AKT/ERK pathway

It has been reported that CXCL11 binds to CXCR3 to regulate immune cell migration, differentiation, and activation [27,28]. To elucidate whether CXCR3 is involved in the effects of CXCL11 from senescent HUVEC on migratory activity, we treated MDA-MB-231 cells with CXCR3 Si and HUVEC with CXCL11 Si. CXCR3 and CXCL11 levels were

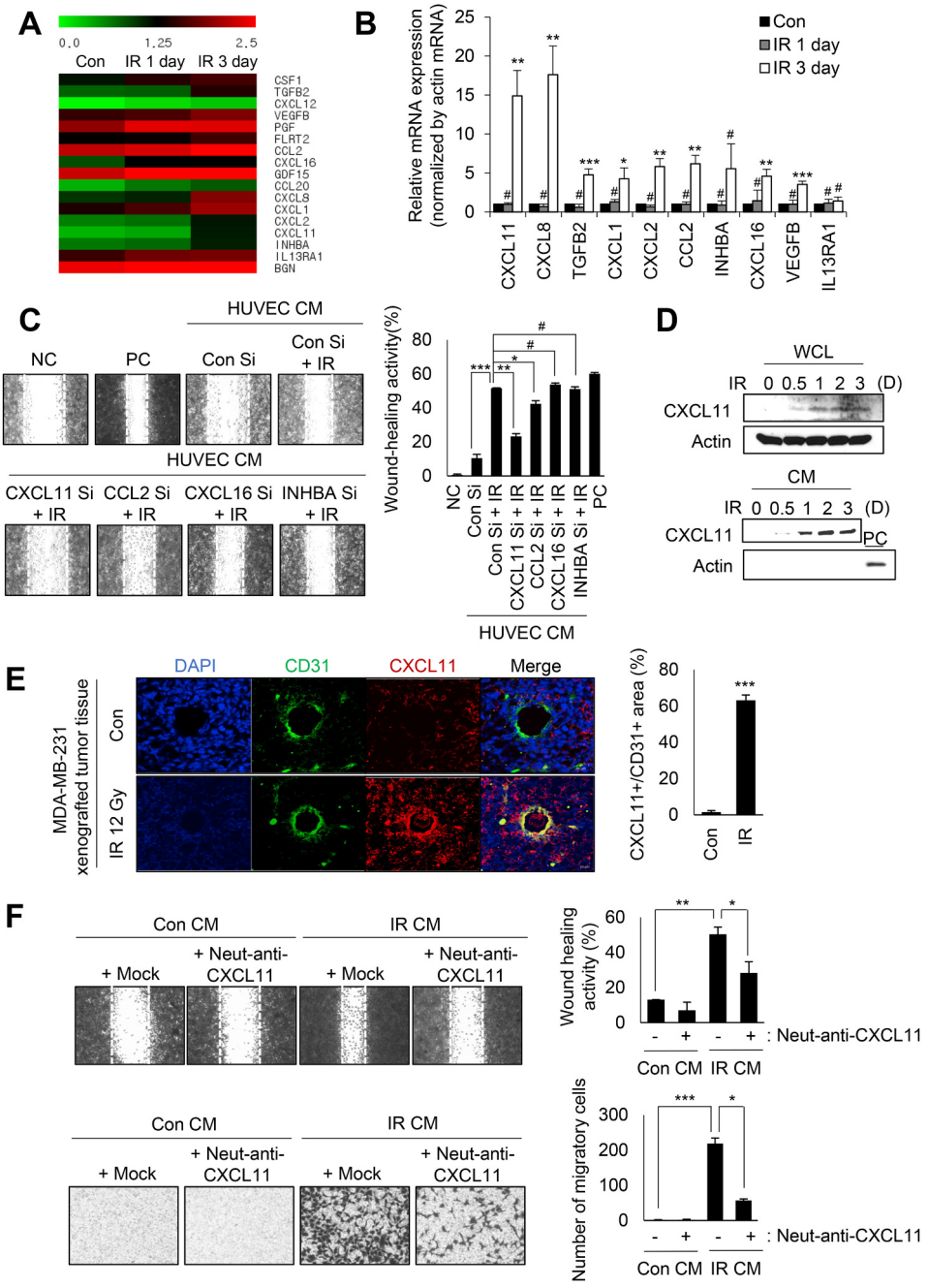

Fig. 3. Analysis of cytokines from IR-induced senescent HUVEC. (A) Identification of cytokine-related genes that are differentially expressed in IR-induced senescent HUVEC. (B) Validation of the differences in the mRNA expression levels of these cytokine-related genes, as assessed by qRT-PCR. (C) Analysis of the migratory activity of HUVEC CM treated-MDA-MB-231 cells. CM was harvested from IR-induced senescent HUVEC that had been transfected with each indicated Si prior to irradiation. Graph indicates quantitative data for the migratory activity. (D) Immunoblot analysis of IR-induced senescent HUVEC. Whole cell lysates (WCL) and CM were obtained from IR-induced senescent HUVEC at the indicated days after irradiation. (E) Immunofluorescence of CD31 and CXCL11 in tumor tissues of xenograft mice injected with MDA-MB-231 cells were locally exposed to 12 Gy of IR. (F) The wound-healing and cell-migratory activities of CM-treated MDA-MB-231 cells. CM was harvested from proliferating (Con)or IR-induced senescent HUVEC, incubated with a neutralizing anti-CXCL11 antibody (Neut-anti-CXCL11) for 4 h, and then applied to MDA-MB-231 cells. For the negative control (NC) and positive control (PC) groups, cells were incubated in serum-free medium and medium containing 1% serum, respectively. The values represent the mean ± SD; n = 3; #P > 0.05; *P <0.05; **P < 0.01; ***P < 0.001.

effectively reduced by the treatment of CXCL11 Si in senescent HUVEC CM and by the treatment of CXCR3 Si in MDA-MB-231 cells (Fig. 4A). The senescent HUVEC CM-induced migratory activity of MDA-MB-231 cells was decreased by the treatment of CXCL11-depleted senescent HUVEC CM and further decreased by the treatment of CXCR3-depleted MDA-MB-231 cells with CXCL11-depleted senescent HUVEC CM (Fig. 4B).

To further define the effect of senescent endothelial cells on cancer cells in a three-dimensional (3D) structure mimicking a tumor microregion, we performed a 3D tumor spheroid invasion assay. The tumor spheroids were generated by co-culture of CXCR3-Si-treated MDA-MB-231 cells with CXCL11-Si treated HUVEC in combination with or without IR- or Doxo-treatment. The invasion area of each spheroid was measured after spheroids were allowed to form for 72 h. We observed that the invasive activity of MDA-MB-231 cells from the tumor spheroid was increased by co-culture with IR- or Doxo-treated HUVEC, and that this effect was decreased by the suppression of CXCR3 in the cancer cells or that of CXCL11 in the endothelial cells (Fig. 4C and D). Together, these results show that CXCR3 depletion in MDA-MB-231 cells and CXCL11 depletion in HUVEC synergistically affect the invasive activity of MDA-MB-231 cells from the tumor spheroid. No off-target effect of CXCL11 was observed in tests performed using three different siRNAs against CXCL11 (Supplementary Fig. S5). We also found that overexpression of CXCL11 rescued the inhibitory effects of CXCL11-depleted senescent HUVEC CM on cell migration, proliferation, and ERK activity (Supplementary Fig. S6).

To know which signaling molecule involves in CXCL11-mediated cancer cell proliferation and metastasis, we examined AKT and ERK activation related with the migratory activity of MDA-MB-231 cells treated with senescent HUVEC CM. We treated MDA-MB-231 cells with IR- or Doxo-induced senescent HUVEC CM and analyzed the phosphorylation of AKT and ERK by immunoblotting (Fig. 5A and B). We observed that AKT phosphorylation was not significantly changed, but ERK phosphorylation was dramatically increased under both of these experimental conditions. When we treated MDA-MB-231 cells with the ERK inhibitor, U0126, prior to applying senescent CM, the wound-healing and migratory activities of these cells were evidently decreased compared to those of cells treated with senescent CM alone (Fig. 5C). When we applied CXCL11-depleted senescent HUVEC CM to MDA-MB-231 cells or senescent HUVEC CM to CXCR3-depleted MDA-MB-231 cells, we found that the relative cell numbers and ERK activation were decreased under both experimental conditions (Fig. 5D and E, lane 4 and 6). Furthermore, when we applied CXCL11-depleted senescent HUVEC CM to CXCR3-depleted MDA-MB-231 cells, the relative cell numbers and ERK activation were further decreased (Fig. 5D and E, lane 8). Together, these results indicate that CXCL11 secreted from senescent

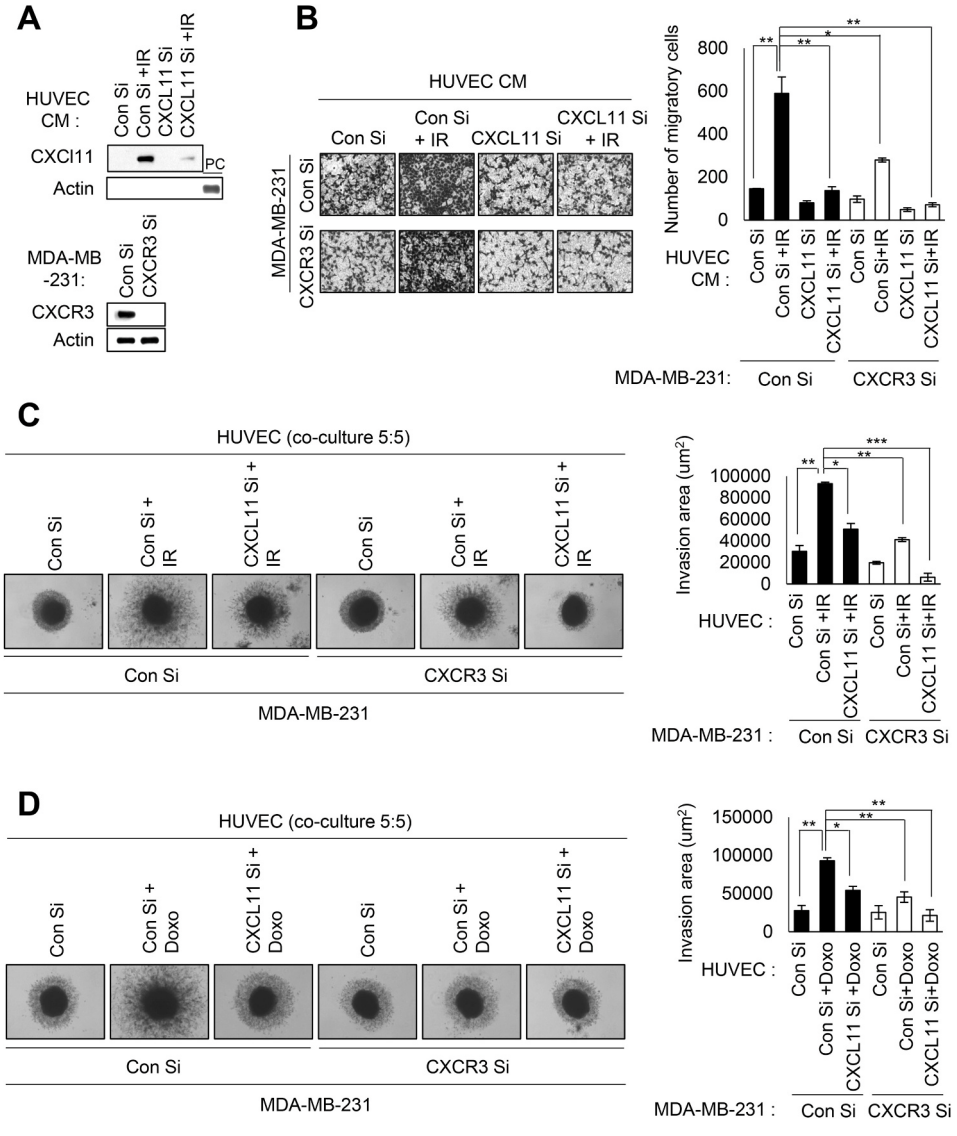

Fig. 4. CXCL11 from senescent HUVEC CM promotes the migratory and invasive activities of MDA-MB-231 cells through the CXCR3 receptor. (A, B) CM from HUVEC transfected with CXCL11 Si prior to IR exposure and cell lysates from MDA-MB-231 cells transfected with CXCR3 Si were subjected to Western blot analysis (A) and was applied to MD-MB-231 cells that had been transfected with Con Si or CXCR3 Si, and the migration activity of the MDA-MB-231 cells was assessed (B). (C, D) Con Si- or CXCR3 Si-treated MDA-MB-231 cells were co-cultured with either IR (C) or Doxo (D)-treated HUVEC transfected with either Con Si or CXCL11 Si prior to IR or Doxo treatment, using a spheroid co-culture system. Each spheroid was loaded with Matrigel and cultivated for 3 days. The invasion area from surface of each spheroid to the boundary of stretched cells was measured. The values represent the mean ± SD; n = 3; *P <0.05; **P < 0.01; ***P < 0.001.

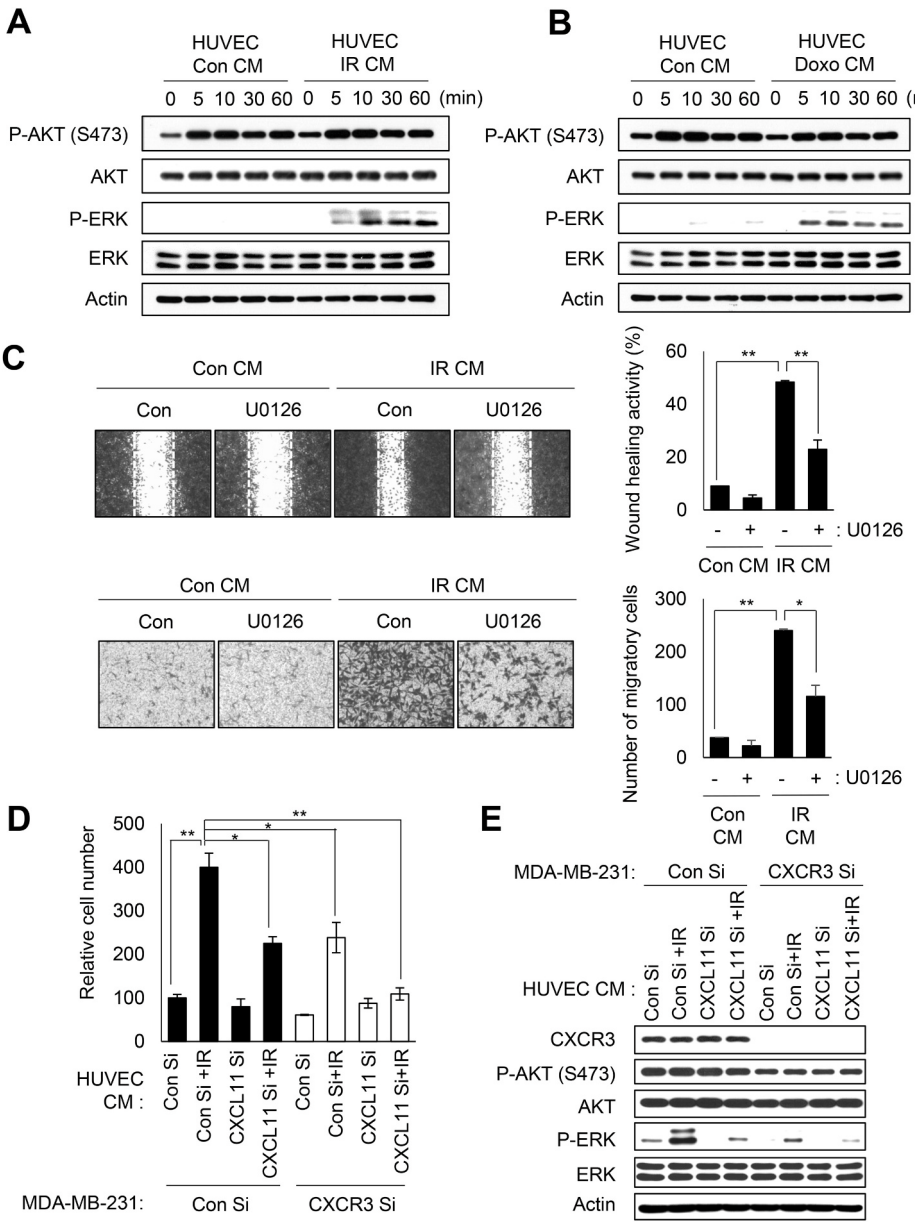

Fig. 5. ERK activation is critical for the ability of senescent HUVEC CM to promote the migratory and invasive activities of MDA-MB-231 cells through the CXCL11-CXCR3 axis. (A, B) CM from proliferating (Con), IR-induced (IR) (A) or Doxo-induced (Doxo) (B) senescent HUVEC was applied to MDA-MB-231 cells and Immunoblot analyses were performed at the indicated times. (C) The ERK inhibitor, U0126 (10 μM), was applied to MDA-MB-231 cells for 1 h before the cells were treated with Con CM or IR CM and assessed for their wound-healing and cell-migratory activities. (D, E) Relative cell numbers (D) and Immunoblot analysis (E) of MDA-MB-231 cells that were transfected with CXCR3 Si treated with CM harvested from proliferating (Con) and IR-induced (IR) senescent HUVEC transfected with CXCL11 Si. The values represent the mean ± SD; n = 3; *P <0.05; **P < 0.01.

HUVEC CM binds to CXCR3 of MDA-MB-231 cells and promotes their migratory and invasive activities through the ERK pathway. To investigate the effect of CXCL11 secreted from senescent HUVEC on other types of breast cancer cells, we tested an ER + cell line (MCF7) and two triple-negative breast cancer cell lines (MDA-MB-453 and HCC70). Senescent HUVEC CM treatment induced cell proliferation and migration in three additional breast cancer cell lines: MCF7, MDA-MB-453, and HCC70 (Supplementary Fig. S7). The cell proliferation and migratory activities of these three breast cancer cell lines were reduced by the application of CXCL11-depleted senescent HUVEC CM. The ability of IR-induced (IR) senescent HUVEC CM to increase ERK and AKT phosphorylation was decreased by CXCL11-depleted senescent HUVEC CM in MCF7 and HCC cells. In contrast, MDA-MB-453 cells showed decreased phosphorylation of AKT, but not ERK, following the application of CXCL11-depleted IR HUVEC CM (Supplementary Fig. S7). Together, our findings comprehensively show that CXCL11 from the senescent HUVEC CM increases the relative cell number and migration activity of every tested breast cancer cell line through the activity regulation of either AKT or ERK.

To examine the clinical relevance of CXCL11 and CXCR3, we evaluated their expression levels in breast cancer patient tissues using the GEPIA portal (http://gepia.cancer-pku.cn/). Breast cancer patients with overexpression of CXCL11 and CXCR3 displayed a decreased survival probability compared to those with low-level expression of CXCL11 and CXCR3 (Supplementary Figs. S8A–B). We also observed a positive correlation between the expression levels of CXCL11 and CXCR3 in breast cancer patient tissues (Supplementary Fig. S8C).

3.5. *CXCL11 from senescent HUVEC promotes tumor growth through ERK activation in a xenograft mouse model*

We found that the proliferation, migration, and invasion of MDA-MB-231 cells were primarily affected by CXCL11 secreted from therapy-induced senescent HUVEC *in vitro*. To explore the effect of CXCL11 secreted from senescent endothelial cells *in vivo*, we performed a xenograft tumor growth assay. MDA-MB-231 cells were injected subcutaneously into 5-week-old nude mice to form xenograft tumors. When the tumor volume reached 50 mm^3, three different HUVEC CMs (No IR + Con Si-, IR + Con Si-, IR + CXCL11 Si-treated HUVEC CM) were injected intratumorally to the xenograft tumor tissues. Whereas the growth of

xenograft tumors was significantly increased following injection of IR-exposed senescent (IR + Con Si treated) HUVEC CM, such tumor growth effect was dramatically decreased following injection of IR + CXCL11 Si-treated (senescent) HUVEC CM (Fig. 6A–C). Similarly, western blot analysis of tumor tissues revealed that ERK phosphorylation was significantly increased by IR-exposed HUVEC CM, but not by IR + CXCL11 Si-treated HUVEC CM (Fig. 6D). In contrast, there was little between-group difference in the AKT phosphorylation of tumor tissues (Fig. 6D). Consistent results were obtained when we used immunostaining to examine ERK and AKT phosphorylation in tumor tissues injected with CM from the three different experimental conditions (Fig. 6E). Collectively, these data demonstrate that CXCL11 secreted from IR-induced senescent HUVEC promotes tumor growth through ERK activation in an *in vivo* tumor xenograft mouse model.

4. Discussion

Therapy-induced senescence (TIS) is a well-founded response to conventional cancer therapy; it has been regarded as a favorable consequence of cancer treatment and a basis for the development of novel remedies that promote a cytostatic response in cancer cells [29]. However, numerous lines of evidence have raised the concern that TIS could cause an unexpected outcome of therapy by supplying a mechanism for tumor dormancy and disease recurrence [30]. Recent studies strongly suggest that senescence is associated with a complicated reprogramming process that can ultimately promote cancer stemness and set off a more aggressive phenotype [31]. The SASP is a highly conserved reaction to genotoxic stress that develops in senescent fibroblasts in culture, epithelial cells *in vivo*, and cancer cells exposed to DNA-damaging therapeutic agents [5]. Senescent cells go through extensive alterations in gene expression; these changes are seen not only in genes related to cell cycle regulation, but also trigger enhanced expression of a spectrum of secreted proteins [32,33]. Specifically, senescent cells have been documented to secrete a spectrum of pro-inflammatory chemokines and cytokines that have paracrine tumor-promoting effects [33]. For example, senescent fibroblasts can augment tumor xenograft growth in animals and promote pre-neoplastic cellular growth both by direct cellular contact and by secreting soluble factors near the tumor cells [20]. Irrespective of how senescence is induced, senescent fibroblasts can expedite tumorigenesis [20]. This suggests that chemotherapy and radiation might also promote cancer development in the TME via the induction of senescence. Various

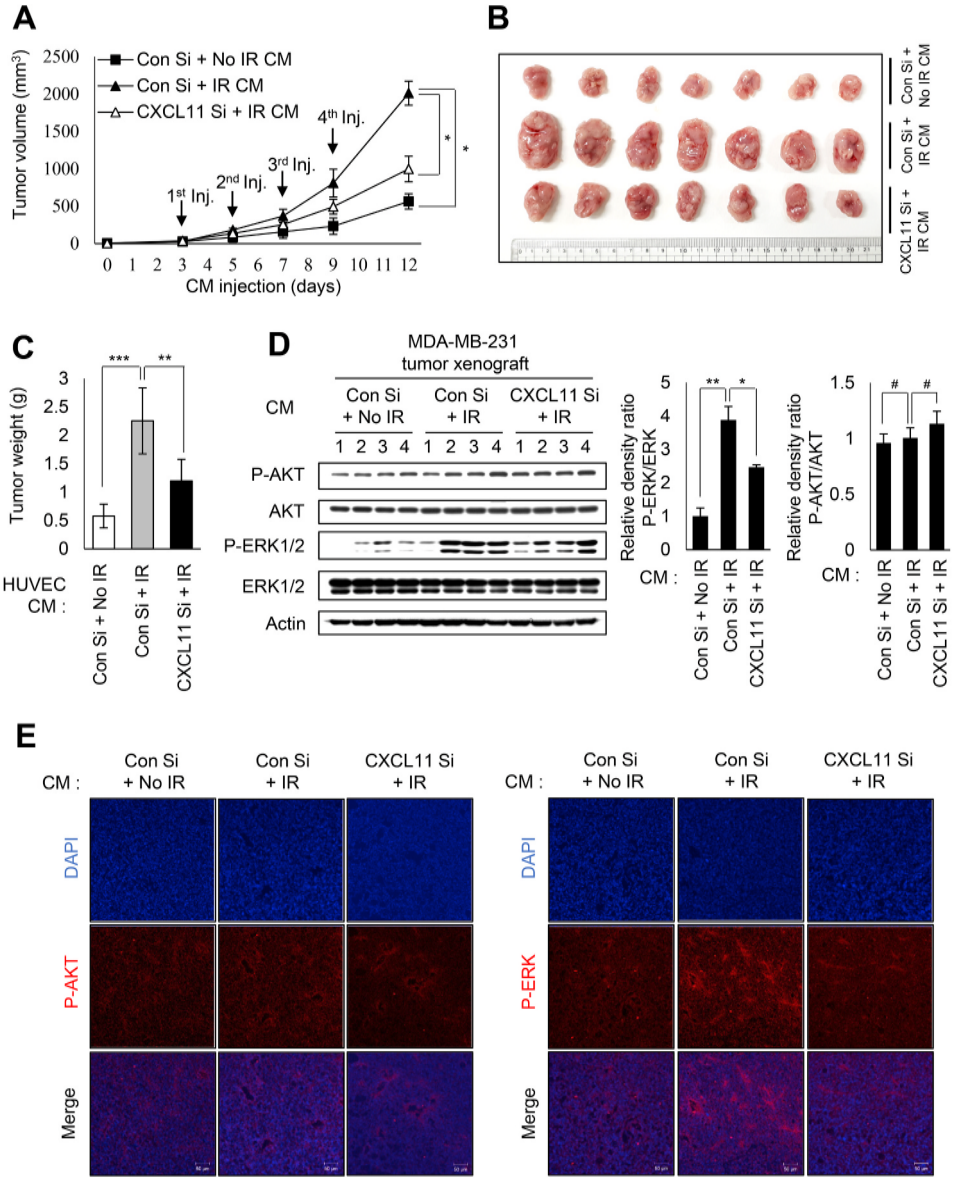

Fig. 6. CXCL11 secreted from senescent HUVEC promotes tumor growth in xenograft mice through ERK activation. (A) Tumor growth was measured at the indicated times in xenograft mice. MDA-MB-231 cells (2 × 106) were injected subcutaneously into male nude mice. When the tumor volume reached 50 mm3, mice were intratumorally injected every other day with CM harvested from proliferating (Con) or IR-exposed HUVEC with or without CXCL11 Si treatment. Error bars represent mean ± SEM (n = 7). (B, C) Photographs (B) and the average weights (C) of tumors harvested at the endpoint. (D, E) Immunoblot analysis (D) and immunostaining (E) for P-AKT (S473), AKT, P-ERK1/2, and ERK1/2 in tumor lysates and sections from HUVEC CM-injected tumors, respectively. The values represent the mean ± SD; n = 3; #P > 0.05; *P <0.05; **P < 0.01; ***P < 0.001You can also find the caption in the attached file as below.

elements of the SASP are related to induction of the EMT, which increases the invasiveness of the developing epithelial tumor [34]. In addition, the SASP is strongly involved accelerating the cancer stem cell-like phenotype seen following the exposure of cancer cells to DNA-damaging conditions [35]. This tumor stromal cell-mediated paracrine effect is detrimental and influences tumor behavior, the response to cancer treatment, and the overall therapy outcome. However, the non-cell-autonomous effects of the chemotherapy-induced SASP on the TME are not yet fully understood. In particular, although endothelial cells are very important for cancer metastasis, most of the studies on the factors secreted from endothelial cells have been performed mainly in diseases such as thrombosis or atherosclerosis; only a few studies have examined how they affect the TME. In the present study, therefore, we triggered senescence in various endothelial cells (including HUVEC, HMVEC, and ECFC) using radiation or anti-cancer drugs and examined how their SASP affected the TME. We found that SASP from therapy-induced senescent endothelial cells affected the proliferation, migration, and invasion of a human breast cancer cell line (MDA-MB-231). Interestingly, however, the SASP from therapy-induced senescent endothelial cells had little effect on the proliferation, migration, or wound-healing activities of a normal breast epithelial cell line (MCF-10A). This suggests that cancer cells might be more sensitive than normal cells in responding to SASP from senescent endothelial cells and might therefore be more likely to acquire an ability to escape from the original tumor bed when endothelial cells undergo senescence.

To elucidate which cytokine(s) from senescent HUVEC had the strongest influence on the TME, we identified the cytokines that showed the most differential expression between therapy-induced senescent and control HUVEC. We found that CXCL11 plays critical roles in promoting the proliferative, migratory, and invasive activities of MDA-MB-231 cells via ERK activation. We demonstrated that CXCL11 affects the aggressive features of cancer cells both *in vitro* and in an *in vivo* xenograft mouse model. The CXC chemokines, CXCL9, -10, and −11, are IFNγ-induced small secretory proteins that are expressed and secreted by leukocytes, as well as epithelial, endothelial, and stromal cells [36]. These chemokines interact with the G protein complex receptor, CXCR3, apply signaling effects in a paracrine or autocrine fashion [37,38], and are well-known chemo-attractants for activated CXCR3+ T cells [36]. Recent work showed that elevated expressions of these chemokines are related with advanced-stage cancer in malignant melanoma, ovarian carcinoma, and B-cell lymphoma [39–41]. In addition, the IFNγ-induced production of CXCL9, -10, and −11 in human neonatal foreskin keratinocytes is reportedly increased during inflammatory dermatoses, such as psoriasis [42–44]. CXCL11 is also known as interferon-inducible T-cell alpha chemoattractant (I-TAC) or interferon-gamma-inducible protein 9 (IP-9) [45]. Among CXCL9, -10, and −11, CXCL11 shows the strongest binding affinity for CXCR3 [46] and uses a different binding domain on CXCR3 relative to those recognized by CXCL9 and -10 [47]. Several studies have shown that the CXCL11–CXCR3 axis plays an important role within the TME [27,48]. A study showed that the tumor growth and invasiveness of human colon adenocarcinoma was augmented after injection of CXCL11 to the TME [49]. Suppressing CXCL11 in colorectal cancer tissues has been shown to decrease tumor cell growth and metastasis [50]. The enhancement of CXCL11 in hepatocellular carcinoma cells is reportedly involved in the upregulation of stem cell-related genes, along with the autocrine axis-related acquisition/maintenance of self-renewal and tumorigenic characteristics among tumor-initiating cells [51]. In contrast, tumors exhibited higher expression of CXCL11 reduced tumor progression by increasing the infiltration of $CD8^+$ T cells and positively correlation with prolonged overall survival in NSCLC (Non-Small Cell Lung Cancer) patients [52], and an analysis of the Human Protein Atlas database (www.proteinatlas.org) revealed that high CXCL11 levels prolonged survival in ovarian cancer patients (Supplementary Fig. S8). In the present study, we demonstrate for the first time that CXCL11 from senescent endothelial cells contributes to the aggressive features of cancer cells through binding CXCR3 and activating ERK.

Overall, therapy-induced endothelial cell senescence has detrimental effects on the success of cancer therapy. To overcome the side effects of TIS, researchers need to consider the interaction between the stromal cell SASP and cancer cells in the TME. We hypothesize that inhibition of CXCL11 secretion from senescent endothelial cells could potentially be combined with conventional cancer therapy to alleviate the deleterious effects of therapy-induced endothelial cell senescence.

Declaration of competing interest

The authors declare no conflict of interest.

CRediT authorship contribution statement

Hyun Jung Hwang: Investigation, Writing - original draft, Writing - review & editing, Validation, Visualization. **Ye-Rim Lee:** Conceptualization, Investigation, Validation. **Donghee Kang:** Conceptualization, Writing - review & editing. **Hyung Chul Lee:** Conceptualization, Writing - review & editing. **Haeng Ran Seo:** Conceptualization, Writing - review & editing. **Ji-Kan Ryu:** Conceptualization, Writing - review & editing. **Yong-Nyun Kim:** Conceptualization, Writing - review & editing. **Young-Gyu Ko:** Conceptualization, Writing - review & editing. **Heon Joo Park:** Conceptualization, Writing - review & editing. **Jae-Seon Lee:** Data curation, Writing - original draft, Writing - review & editing, Supervision, Project administration, Funding acquisition.

Acknowledgements

The ECFC were kindly gifted by Prof. Man Ryul Lee (Soonchunhyang University, Cheonan, Korea). This work was supported by grants to JSL from MRC (2014R1A5A2009392) and the Basic Research Science Program (2020R1A2B5B02002375) through the National Research Foundation (NRF) funded by the Korean government (MSIT).

Appendix A. Supplementary data

Supplementary data to this article can be found online at https://doi.org/10.1016/j.canlet.2020.06.019.

References

[1] L. Hayflick, P.S. Moorhead, The serial cultivation of human diploid cell strains, Exp. Cell Res. 25 (1961) 585–621.
[2] L. Hayflick, The limited in vitro lifetime of human diploid cell strains, Exp. Cell Res. 37 (1965) 614–636.
[3] T. Kuilman, C. Michaloglou, W.J. Mooi, D.S. Peeper, The essence of senescence, Genes Dev. 24 (2010) 2463–2479.
[4] E.P. Crowe, T. Nacarelli, A. Bitto, C. Lerner, C. Sell, C. Torres, Detecting senescence: methods and approaches, Methods Mol. Biol. 1170 (2014) 425–445.
[5] J.P. Coppe, P.Y. Desprez, A. Krtolica, J. Campisi, The senescence-associated secretory phenotype: the dark side of tumor suppression, Annu. Rev. Pathol. 5 (2010) 99–118.
[6] A. Freund, A.V. Orjalo, P.Y. Desprez, J. Campisi, Inflammatory networks during cellular senescence: causes and consequences, Trends Mol. Med. 16 (2010) 238–246.
[7] C. Gabay, Interleukin-6 and chronic inflammation, Arthritis Res. Ther. 8 (2006) S3.
[8] S.L. Kunkel, T. Standiford, K. Kasahara, R.M. Strieter, Interleukin-8 (IL-8): the major neutrophil chemotactic factor in the lung, Exp. Lung Res. 17 (1991) 17–23.
[9] Y.H. Kim, Y.W. Choi, J. Lee, E.Y. Soh, J.H. Kim, T.J. Park, Senescent tumor cells lead the collective invasion in thyroid cancer, Nat. Commun. 8 (2017) 15208.
[10] S. Parrinello, J.P. Coppe, A. Krtolica, J. Campisi, Stromal-epithelial interactions in aging and cancer: senescent fibroblasts alter epithelial cell differentiation, J. Cell Sci. 118 (2005) 485–496.
[11] B.G. Childs, M. Durik, D.J. Baker, J.M. van Deursen, Cellular senescence in aging and age-related disease: from mechanisms to therapy, Nat. Med. 21 (2015) 1424–1435.
[12] A. Prieur, D.S. Peeper, Cellular senescence in vivo: a barrier to tumorigenesis, Curr. Opin. Cell Biol. 20 (2008) 150–155.
[13] E. Sikora, A. Bielak-Zmijewska, G. Mosieniak, Cellular senescence in ageing, age-related disease and longevity, Curr. Vasc. Pharmacol. 12 (2014) 698–706.
[14] M. Demaria, N. Ohtani, S.A. Youssef, F. Rodier, W. Toussaint, J.R. Mitchell, R. M. Laberge, J. Vijg, H. Van Steeg, M.E. Dollé, J.H. Hoeijmakers, A. de Bruin,

E. Hara, J. Campisi, An essential role for senescent cells in optimal wound healing through secretion of PDGF-AA, Dev. Cell 31 (2014) 722–733.
[15] D. Muñoz-Espín, M. Serrano, Cellular senescence: from physiology to pathology, Nat. Rev. Mol. Cell Biol. 15 (2014) 482–496.
[16] Y. Ovadya, V. Krizhanovsky, Senescent cells: SASPected drivers of age-related pathologies, Biogerontology 15 (2014) 627–642.
[17] D.J. Baker, C. Perez-Terzic, F. Jin, K.S. Pitel, N.J. Niederländer, K. Jeganathan, S. Yamada, S. Reyes, L. Rowe, H.J. Hiddinga, N.L. Eberhardt, A. Terzic, J.M. van Deursen, Opposing roles for p16Ink4a and p19Arf in senescence and ageing caused by BubR1 insufficiency, Nat. Cell Biol. 10 (2008) 825–836.
[18] D.J. Baker, T. Wijshake, T. Tchkonia, N.K. LeBrasseur, B.G. Childs, B. van de Sluis, J.L. Kirkland, J.M. van Deursen, Clearance of p16Ink4a-positive senescent cells delays ageing-associated disorders, Nature 479 (2011) 232–236.
[19] M. Collado, J. Gil, A. Efeyan, Tumour biology: senescence in premalignant tumours, Nature 436 (2005) 642.
[20] A. Krtolica, S. Parrinello, S. Lockett, P.Y. Desprez, J. Campisi, Senescent fibroblasts promote epithelial cell growth and tumorigenesis: a link between cancer and aging, Proc. Natl. Acad. Sci. U. S. A. 98 (2001) 12072–12077.
[21] G. Lorusso, C. Rüegg, The tumor microenvironment and its contribution to tumor evolution toward metastasis, Histochem. Cell Biol. 130 (2008) 1091–1103.
[22] M.R. Junttila, F.J. de Sauvage, Influence of tumour micro-environment heterogeneity on therapeutic response, Nature 501 (2013) 346–354.
[23] L. Akkari, J.A. Joyce, Microenvironmental InterFereNce of metabolism regulates chemosensitivity, Cell Res. 26 (2016) 867–868.
[24] K.M. Bussard, L. Mutkus, K. Stumpf, C. Gomez-Manzano, F.C. Marini, Tumor-associated stromal cells as key contributors to the tumor microenvironment, Breast Cancer Res. 18 (2016) 84.
[25] Y. Yuan, Y.C. Jiang, C.K. Sun, Q.M. Chen, Role of the tumor microenvironment in tumor progression and the clinical applications, Oncol. Rep. 35 (2016) 2499–2515.
[26] B.C. Kim, H.J. Yoo, H.C. Lee, K.A. Kang, S.H. Jung, H.J. Lee, et al., Evaluation of premature senescence and senescence biomarkers in carcinoma cells and xenograft mice exposed to single or fractionated irradiation, Oncol. Rep. 31 (2014) 2229–2235.
[27] R. Tokunaga, W. Zhang, M. Naseem, A. Puccini, M.D. Berger, S. Soni, M. McSkane, H. Baba, H.J. Lenz, CXCL9, CXCL10, CXCL11/CXCR3 axis for immune activation - a target for novel cancer therapy, Canc. Treat Rev. 63 (2018) 40–47.
[28] Anup Kumar Singh, Rakesh Kumar Arya, Arun Kumar Trivedi, Sabyasachi Sanyal, Rathindranath Baral, Dormond Olivier, David M. Briscoe, Dipak Datta, Chemokine receptor trio: CXCR3, CXCR4 and CXCR7 crosstalk via CXCL11 and CXCL12, Cytokine Growth Factor Rev. 24 (2013) 41–49.
[29] J.A. Ewald, J.A. Desotelle, G. Wilding, D.F. Jarrard, Therapy-induced senescence in cancer, J. Natl. Cancer Inst. 102 (2010) 1536–1546.
[30] M. Demaria, M.N. O'Leary, J. Chang, L. Shao, S. Liu, F. Alimirah, K. Koenig, C. Le, N. Mitin, A.M. Deal, S. Alston, E.C. Academia, S. Kilmarx, A. Valdovinos, B. Wang, A. de Bruin, B.K. Kennedy, S. Melov, D. Zhou, N.E. Sharpless, H. Muss, J. Campisi, Cellular senescence promotes adverse effects of chemotherapy and cancer relapse, Canc. Discov. 7 (2017) 165–176.
[31] M. Milanovic, D.N.Y. Fan, D. Belenki, J.H.M. Däbritz, Z. Zhao, Y. Yu, J.R. Dörr, L. Dimitrova, D. Lenze, I.A. Monteiro Barbosa, M.A. Mendoza-Parra, T. Kanashova, M. Metzner, K. Pardon, M. Reimann, A. Trumpp, B. Dörken, J. Zuber, H. Gronemeyer, M. Hummel, G. Dittmar, S. Lee, C.A. Schmitt, Senescence-associated reprogramming promotes cancer stemness, Nature 553 (2018) 96–100.
[32] H. Zhang, K. Pan, S.N. Cohen, Senescence-specific gene expression fingerprints reveal cell-type-dependent physical clustering of up-regulated chromosomal loci, Proc. Natl. Acad. Sci. U. S. A. 100 (2003) 3251–3256.
[33] J.C. Acosta, A. Banito, T. Wuestefeld, A. Georgilis, P. Janich, J.P. Morton, D. Athineos, T.W. Kang, F. Lasitschka, M. Andrulis, G. Pascual, K.J. Morris, S. Khan, H. Jin, G. Dharmalingam, A.P. Snijders, T. Carroll, D. Capper, C. Pritchard, G. J. Inman, T. Longerich, O.J. Sansom, S.A. Benitah, L. Zender, J. Gil, A complex secretory program orchestrated by the inflammasome controls paracrine senescence, Nat. Cell Biol. 15 (2013) 978–990.
[34] R. Laberge, P. Awad, J. Campisi, P. Desprez, Epithelial-mesenchymal transition induced by senescent fibroblasts, Cancer Microenviron 5 (2012) 39–44.
[35] J. Cahu, S. Bustany, B. Sola, Senescence-associated secretory phenotype favors the emergence of cancer stem-like cells, Cell Death Dis. 3 (2012) e446–448.
[36] A. Pellegrino, F. Antonaci, F. Russo, F. Merchionne, D. Ribatti, A. Vacca, F. Dammacco, CXCR3-binding chemokines in multiple myeloma, Canc. Lett. 207 (2004) 221–227.
[37] M. Baggiolini, Chemokines in pathology and medicine, J. Intern. Med. 250 (2001) 91–104.
[38] R.A. Hall, R.T. Premont, R.J. Lefkowitz, Heptahelical receptor signaling: beyond the G protein paradigm, J. Cell Biol. 145 (1999) 927–932.
[39] M. Furuya, T. Suyama, H. Usui, Y. Kasuya, M. Nishiyama, N. Tanaka, I. Ishiwata, Y. Nagai, M. Shozu, S. Kimura, Up-regulation of CXC chemokines and their receptors: implications for proinflammatory microenvironments of ovarian carcinomas and endometriosis, Hum. Pathol. 38 (2007) 1676–1687.
[40] D. Jones, R.J. Benjamin, A. Shahsafaei, D.M. Dorfman, The chemokine receptor CXCR3 is expressed in a subset of B-cell lymphomas and is a marker of B-cell chronic lymphocytic leukemia, Blood 95 (2000) 627–632.
[41] C. Monteagudo, J.M. Martin, E. Jorda, A. Llombart-Bosch, CXCR3 chemokine receptor immunoreactivity in primary cutaneous malignant melanoma: correlation with clinicopathological prognostic factors, J. Clin. Pathol. 60 (2007) 596–599.
[42] N. Kanda, T. Shimizu, Y. Tada, S. Watanabe, IL-18 enhances IFN-gamma-induced production of CXCL9. CXCL10, and CXCL11 in human keratinocytes, Eur. J. Immunol. 37 (2007) 338–350.
[43] N. Kanda, S. Watanabe, Prolactin enhances interferon-gamma-induced production of CXC ligand 9 (CXCL9). CXCL10, and CXCL11 in human keratinocytes, Endocrinology 148 (2007) 2317–2325.
[44] J.B. Mee, C.M. Johnson, N. Morar, F. Burslem, R.W. Groves, The psoriatic transcriptome closely resembles that induced by interleukin-1 in cultured keratinocytes: dominance of innate immune responses in psoriasis, Am. J. Pathol. 171 (2007) 32–42.
[45] M.R. Rani, G.R. Foster, S. Leung, D. Leaman, G.R. Stark, R.M. Ransohoff, Characterization of beta-R1, a gene that is selectively induced by interferon beta (IFN-beta) compared with IFN-alpha, J. Biol. Chem. 271 (1996) 22878–22884.
[46] Y. Weng, S.J. Siciliano, K.E. Waldburger, A. Sirotina-Meisher, M.J. Staruch, B. L. Daugherty, et al., Binding and functional properties of recombinant and endogenous CXCR3 chemokine receptors, J. Biol. Chem. 273 (1998) 18288–18291.
[47] R.A. Colvin, G.S. Campanella, J. Sun, A. D, Luster Intracellular domains of CXCR3 that mediate CXCL9, CXCL10, and CXCL11 function, J. Biol. Chem. 279 (2004) 30219–30227.
[48] N. Reynders, D. Abboud, A. Baragli, M.Z. Noman, B. Rogister, S.P. Niclou, N. Heveker, B. Janji, J. Hanson, M. Szpakowska, A. Chevigné, The distinct roles of CXCR3 variants and their ligands in the tumor microenvironment, Cells 18 (2019) 8.
[49] K. Rupertus, J. Sinistra, C. Scheuer, R.M. Nickels, M.K. Schilling, M.D. Menger, O. Kollmar, Interaction of the chemokines I-TAC (CXCL11) and SDF-1 (CXCL12) in the regulation of tumor angiogenesis of colorectal cancer, Clin. Exp. Metastasis 31 (2014) 447–459.
[50] Y.J. Gao, S.L. De Lin Liu, G.F. Yuan, L. Li, H.Y. Zhu, G.Y. Cao, Down-regulation of cXcl11 inhibits colorectal cancer cell growth and epithelial-mesenchymal transition, OncoTargets Ther. 11 (2018) 7333–7343.
[51] Y. Zhang, W. Zhao, S. Li, M. Lv, X. Yang, M. Li, Z. Zhang, CXCL11 promotes self-renewal and tumorigenicity of α2δ1+ liver tumor-initiating cells through CXCR3/ERK1/2 signaling, Canc. Lett. 449 (2019) 163–171.
[52] Q. Gao, S. Wang, X. Chen, S. Cheng, Z. Zhang, F. Li, L. Huang, Y. Yang, B. Zhou, D. Yue, D. Wang, L. Cao, N.R. Maimela, B. Zhang, J. Yu, L. Wang, Y. Zhang, Cancer-cell-secreted CXCL11 promoted CD8+ T cells infiltration through docetaxel-induced-release of HMGB1 in NSCLC, J Immunother Cancer 7 (2019) 42.